Rendiconti Lincei. Scienze Fisiche e Naturali (2022) 33:537–553
https://doi.org/10.1007/s12210-022-01076-7

RESEARCH PAPER

Biomediated nanosized ZnS using *Ulva fasciata* and *Citrus japonica*: A new bio-photocatalyst for textile wastewater treatment

Asmaa El Nady[1] · Rateb N. Abbas[2] · Noha M. Sorour[3]

Received: 6 January 2022 / Accepted: 28 May 2022 / Published online: 28 July 2022

Abstract

The aquatic ecosystems face excessive stress and depletion due to many pollutants impacting water quality. Biosynthesis of nanoparticles (NPs) using the green route represents a cost-effectively and eco-friendly approach, with significant applicability in various fields. In this regard, ZnS-NPs with improved photocatalytic and antimicrobial activities were biosynthesized for the first time from *Ulva fasciata* and *Citrus japonica* aqueous extracts. Biosynthesized ZnS-NPs were characterized and compared with chemically synthesized ones using UV–Vis spectroscopy, FTIR, TEM, XRD, and EDAX. TEM micrographs and XRD confirmed the formation of polygonal and spherical-shaped ZnS blend sphalerite nanocrystals with an average diameter between 7 and 31 nm. The optical properties of the produced ZnS-NPs showed higher band-gap energy of 5.63 eV and 4.76 eV for chemically and biosynthesized ZnS-NPs, respectively, as compared to ZnS macromolecules (3.77 eV). Biosynthesized ZnS-NPs showed excellent photocatalytic activity toward textile wastewater and two organic dyes (crystal violet and safranin), with significant degradation efficiency of 82–96.8, 82.5–98.12, and 84–95.9%, respectively. Biosynthesized ZnS-NPs showed high stability up to three subsequent cycles of photodegradation and exhibited promising antimicrobial activity against different Gram-positive and Gram-negative bacteria and *Candida albicans.* Biosynthesized ZnS-NPs have a less cytotoxic effect (IC_{50} > 300 µg/mL) than chemically synthesized ZnS-NPs (IC_{50} 88 µg/mL) on human skin fibroblast normal cell lines. The photocatalytic efficiency of the biosynthesized ZnS-NPs has some advantages, such as non-toxic products, cost-effectiveness, and antimicrobial activity, which give them superiority to be used as a safe bio-photocatalyst for water treatment.

✉ Noha M. Sorour
noha.sorour@mail.mcgill.ca

[1] Research and Development, Scientific Veterinary Center for Research and Training, Sadat City, Egypt

[2] Department of Microbial Biotechnology, Genetic Engineering and Biotechnology Research Institute (GEBRI), University of Sadat City, Sadat City, Egypt 22857/79

[3] Department of Industrial Biotechnology, Genetic Engineering and Biotechnology Research Institute (GEBRI), University of Sadat City, Sadat City, Egypt 22857/79

Graphical abstract

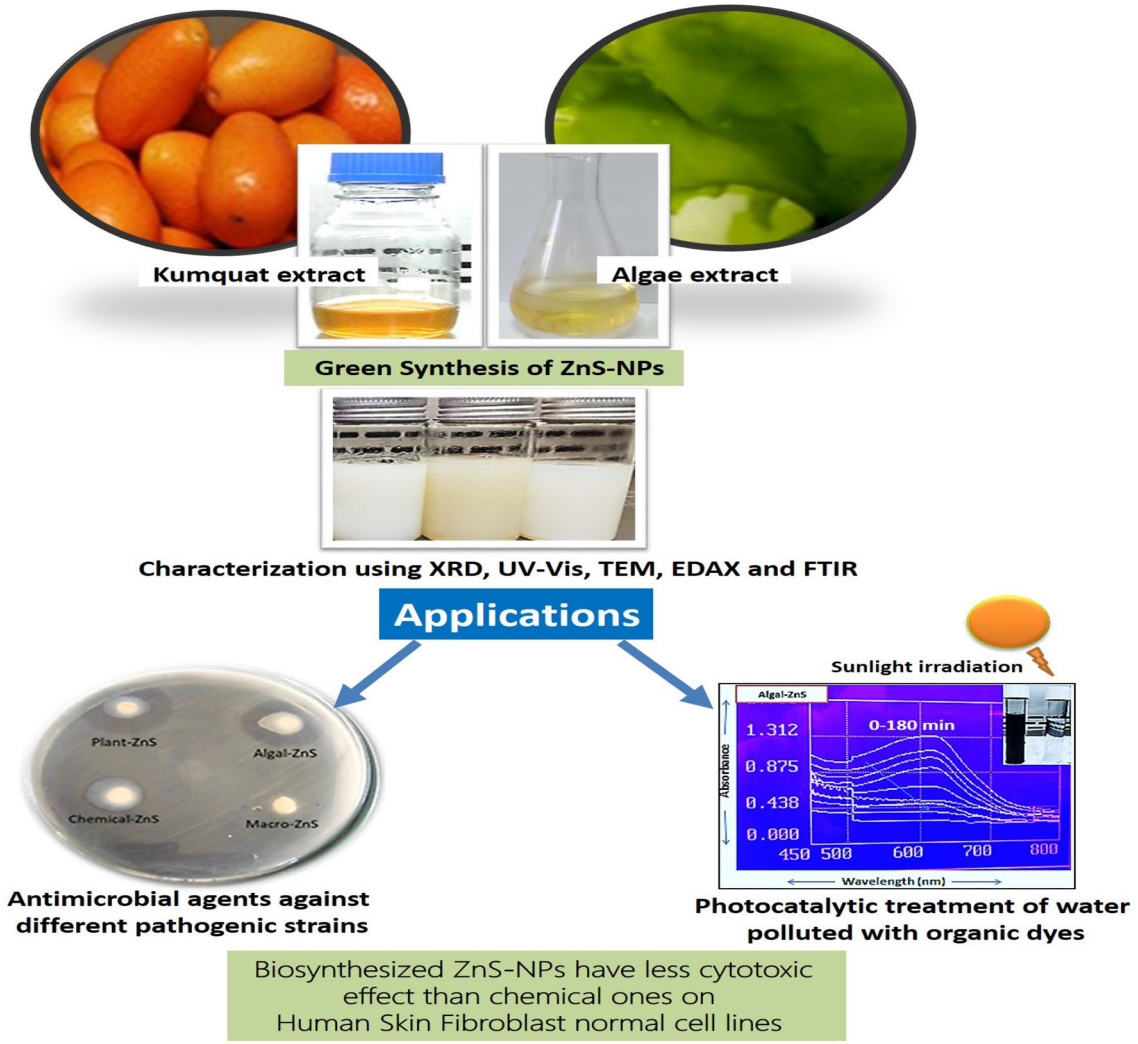

Keywords Bio-photocatalyst · *Citrus japonica* · Nano-ZnS · *Ulva fasciata*

1 Introduction

Environmental pollution is considered a severe problem that continuously increases due to the accumulation of agricultural and industrial wastes (Mansur et al. 2014). Most of the natural potable water sources have been polluted with various toxic materials and pathogenic microorganisms that harmfully affect the aquatic ecosystems (Hassan et al. 2019). The World Bank reported that 17–20% of industrial water pollution arises from textile dyeing (Rafiq et al. 2021). The textile industry causes environmental pollution by accidentally discharging contaminated industrial wastewater into natural water resources. In addition, initiatives such as textiles, paper, and painting use organic dyes, such as azo-dyes, and non-biodegradable products due to their complex structure. However, they are toxic and carcinogenic to living organisms (Ravikumar et al. 2021). Therefore, these dyes adversely impact human health and the environment. As a result, the search for reliable, cost-effective, and innovative methods for water treatment became an international challenge because of the extreme water pollution resources and the continuous deficiency of water resources (Mansur et al. 2014). Many strategies have been developed so far, but green bioremediation is preferable. In this regard, innovative photocatalytic methods have been improved for water treatment (Ambigadevi et al. 2021). Photocatalysis uses sunlight, which is a renewable free energy, an unlimited source of ultraviolet and visible (UV–Vis) radiation, together with a suitable catalyst (e.g., semiconductors) that can destroy pollutants through oxidation–reduction reactions (Rajabi et al.

2020). The photocatalytic process can mineralize hazardous organic chemicals to CO_2, simple mineral acids, and water (Sirajudheen et al. 2021). Significant advantages of the photocatalytic process are no further requirement for secondary removal methods, and no expensive oxidizing chemicals are required (Beydoun et al. 1999).

On the other hand, nanoparticles (NPs) are exciting materials with unique physicochemical features due to the confinement of the charge carriers in the narrow space of its nanocrystal. Nanosized binary chalcogenides which belong to groups II–VI semiconductors, such as ZnS, CdS, and PbS, have gained significant consideration in many applications due to their unique characteristics compared to their bulk counterparts (El-Baz et al. 2016; Ambigadevi et al. 2021). In this respect, ZnS is a valuable semiconductor in some applications, such as electroluminescence, photocatalysis, and biosensors (Dhir 2021). Various chemical and physical methods are used to synthesize nanostructured ZnS (Sadovnikov 2019). However, some chemical and biological methods still have problems, such as use of high temperature and pressure, synthesis cost, hazardous solvents and reagents, and therefore not considered eco-friendly (Chan et al. 2021).

Interestingly, the green synthesis of NPs is a non-toxic, cost-effective, and eco-friendly approach; it is considered the best alternative to physical or chemical methods (Qamar et al. 2019). Few scientific reports for the green synthesis of nanosized ZnS using algae and plants have been reported (Rao et al. 2016; Mani et al. 2018; Alijani et al. 2019; Kannan et al. 2020; Rajabi et al. 2020). In the present study, a simple, reliable, cost-effective green approach for the biosynthesis of ZnS-NPs using aqueous extracts of algae and kumquat was described for the first time. The optical, morphological, and chemical characterization of the produced ZnS-NPs have been studied using UV–Vis, FTIR, XRD, TEM, and EDAX. The antimicrobial activity and the photodegradation efficiency of both the chemically and biosynthesized ZnS-NPs toward textile industrial wastewater and two organic dyes (crystal violet and safranin) have been studied. Also, the cytotoxicity of the produced ZnS-NPs was assessed for biosafety applications.

2 Materials and methods

2.1 Chemicals, culture media, and microorganisms

Na_2S was obtained from Loba Chemie, India. EDTA and $ZnSO_4.7H_2O$ were obtained from El Gomhoria Chemicals co. Ltd, Cairo, Egypt. Nutrient broth and Wickerham media were obtained from Loba Chemie, India. All other chemicals and reagents were bought locally and were of analytical reagent grade. Gram-positive bacteria (*Bacillus subtilis* DSM 5552) were obtained from GEBRI, University of Sadat City (Ahmed et al. 2021), *Staphylococcus aureus* (ATCC 6538) and Gram-negative strains (*Escherichia coli* ATCC 8739, *Klebsiella pneumonia* ATCC 700603, *Acinetobacter baumannii* ATCC 17978), and yeast (*C. albicans* ATCC 10231) were obtained from El-Mabarra Educational Hospital, Alexandria, Egypt.

2.2 Preparation of kumquat peel and *Ulva fasciata* algal aqueous extracts

Citrus japonica fruits were bought from the local market of Sadat City, Minufyia governorate, Egypt. Fresh *C. japonica* (kumquat) fruits peels were washed with tap water followed by distilled water, cut into small pieces, and dried at 40 °C until complete dryness, then powdered using a mechanical grinder. Five grams of powdered *C. japonica* peels were added to 50 mL distilled water in a water bath and heated for 15 min at 50 °C (Reenaa and Menon 2017). The extract was filtered through Whatman No.1 filter paper; the solution was filtered through a 0.45 µm sterile membrane filter and stored at 4 °C. *Ulva fasciata* was collected from shallow water at Abo-Qir shore, Alexandria, Egypt and was identified by Hamouda et al. (2020). Marine algae were washed with fresh seawater to remove the epiphytes, sand, and other extraneous matters. *Ulva fasciata* algae were air-dried under shading away from sunlight and completely dried in the oven at 60 °C. The dried algae were ground to powder using a mechanical grinder. The aqueous algal extract was prepared by adding 1 g of dried algal powder to 100 mL of double-distilled water, boiled for 1 h, filtered through Whatman No.1 filter paper, sterilized using sterile 0.45 µm membrane filter, and stored at 4 °C for further use. All experiments were done under sterilized conditions.

2.3 Chemical synthesis of ZnS-NPs

ZnS-NPs were prepared according to Wadhwani and Jain (2015) using the co-precipitation method. Na_2S and $ZnSO_4.7H_2O$ were used as the Zn^{+2} and S^{+2} sources, respectively. Solutions of 0.1 M $ZnSO_4.7H_2O$, 0.1 M Na_2S, and EDTA (1% w/v) were prepared in double-distilled water. 50 mL of EDTA (1%) and 50 mL of 0.1 M $ZnSO_4.7H_2O$ were mixed and stirred for 30 min to get a homogeneous solution. 0.1 M Na_2S was added dropwise under vigorous stirring for 1 h until the formation of a white precipitate of ZnS-NPs, separated by centrifugation at 6000 rpm for 20 min, washed with double-distilled water, and dried in the oven at 80 °C for 4 h.

2.4 Biological synthesis of ZnS-NPs

ZnS-NPs were biologically synthesized using either 10 mL of *Ulva fasciata* aqueous algal extract (UfaqE) or kumquat aqueous peels extract (KaqPE). Extracts were added separately in reaction vessels to 50 mL of 0.1 M $ZnSO_4.7H_2O$ solution and stirred for 30 min. An appropriate amount of 0.1 M Na_2S was added drop by drop to the reaction mixture under continuous magnetic stirring (1000 rpm) for 1 h. The white colloidal suspension of ZnS-NPs was precipitated, separated, and dried following the method mentioned above.

2.5 Characterization of ZnS-NPs using UV–Vis spectroscopy, FTIR, TEM, XRD, and EDAX

UV–Vis's absorption spectroscopy was used to study the physical characteristics of NPs. The UV–Vis absorbance spectroscopy is also used to monitor the surface plasmon resonance band distinctive for ZnS-NPs from 290 to 500 nm, using the Shimadzu T80 spectrophotometer (China). Band-gap energy (*Eg*) of the chemically and biosynthesized ZnS-NPs was calculated using the Tauc-plot equation (Eyasu et al. 2013):

$$Eg\ (eV)\ =\ 1240/\lambda$$

where *Eg* is the band-gap energy (in electron volts), and λ is the wavelength (nm) at maximum absorption. Fourier transform infrared spectroscopy (FTIR) measurements of ZnS-NPs samples were recorded on an FTIR spectrometer 8000 series, with KBr in the wavenumber region of 4000–400 cm^{-1} at a resolution of 4 cm^{-1}. The size and morphology of the produced ZnS-NPs were investigated by transmission electron microscopy, FETEM, JSM-2100F, JEOL Inc. An aliquot of a colloidal suspension of ZnS-NPs was transmitted onto a carbon-coated copper grid, dried, and scanned at an accelerating voltage of 15 and 200 kV. The size and crystal phase of the dried powdered samples were characterized by powder X-ray diffraction (XRD, Bruker D2 Phaser diffractometer, 2nd Gen.), operating at 30 kV and 10 mA, with Cu anode radiation (1.54060 Å) in the angular range of 10–70°, using continuous scanning 2Θ mode. Energy-dispersive absorption X-ray spectroscopy (EDAX) analysis of ZnS-NPs was done using JEOL JSM-6100 SEM at 20 kV, and modified to conclude the elemental configuration of the sample.

2.6 Photocatalytic activity of the produced ZnS-NPs

The photocatalytic activities of chemically and biosynthesized ZnS-NPs were assessed by measuring the photodegradation of two organic dyes [crystal violet (CV) and safranin (SF)] under sunlight irradiation. CV and SF are water-soluble cationic dyes that were used as model compounds for the oxidation reactions of environmental organic pollutants. As a true model of water pollutants, the photodegradation of industrial wastewater from the local textile factory was also performed using the produced ZnS-NPs as the photocatalyst. The industrial wastewater was collected from Alrobaeia Textile Factory, 6th Industrial region, Sadat City, Minufyia governorate, Egypt. Experiments were performed at room temperature in the quartz-glass cylinder by adding 10 mg of chemically or biosynthesized ZnS-NPs to 100 mL of (1×10^{-5}) M of either CV, SF, or industrial wastewater. Mixed suspensions were stirred in the dark for 30 min to achieve adsorption–desorption equilibrium. The mixed suspensions containing the photocatalyst and the dye were irradiated under sunlight up to 90 min for CV, 180 min for SF, and 160 min for wastewater. On the other hand, 100 mL of industrial wastewater or (1×10^{-5}) M of either CV or SF without the photocatalyst was irradiated under the same conditions as a negative control to study the effect of sunlight only. Two mL samples were collected every 10 min intervals and scanned by UV–Vis spectroscopy to determine the dye concentration according to Beer–Lambert law and calculate the correlation between the absorbance and the dye concentrations at their characteristic maximum absorption wavelengths (λ_{585} for CV, λ_{518} for SF, and λ_{620} for industrial wastewater). The photocatalytic degradation efficiency of the biocatalyst ZnS-NPs was determined using the following equation (Eyasu et al. 2013):

$$\begin{aligned}\text{Degradation efficiency (D\%)} &= \left(1-A_t/A_0\right)\ \times\ 100\\ &= \left(1-C_t/C_0\right)\ \times\ 100,\end{aligned}$$

where A_0 is the absorbance of dye solution at the initial stage (0 min), A_t is the absorbance of dye solution at time 't' of the reaction, and C_0 and C_t are the corresponding dye concentrations, respectively. The recyclability and stability of the synthesized ZnS-NPs were tested. ZnS-NPs were recovered by centrifugation at 6000 rpm for 10 min, washed twice with double-distilled water, and dried at 80 °C for 3 h. The dried powder was used as the photocatalyst for another photodegradation cycle of 100 mL of industrial wastewater, using the above-described method.

2.7 Cytotoxicity assay

The cytotoxic activities of chemically and biologically synthesized ZnS-NPs were assessed on human skin fibroblast (HSF) cell lines. The cell viability was evaluated by sulforhodamine B (SRB) assay at Nawah Scientific Inc. (Cairo, Egypt) based on Skehan et al.'s (1990) method. Cells were preserved in Dulbecco's minimum essential medium

(DMEM) supplemented with 100 U/mL of penicillin, 100 mg/mL of streptomycin, and 10% of heat-inactivated fetal bovine serum in humidified, 5% (v/v) CO_2 atmosphere at 37 °C. Aliquots of 100 µL cell suspension (5×10^3 cells) were plated in 96-well plates and incubated for 24 h. Cells were treated with another aliquot of 100 µL media containing Zn-NPs at concentrations of 0.03–300 µg/mL. After 72 h of Zn-NPs exposure, cells were fixed by replacing media with 150 µL of 10% TCA (trichloroacetic acid) and incubated at 4 °C for 1 h. The TCA solution was removed, and the cells were washed five times with double-distilled H_2O. Aliquots of 70 µL SRB (sulforhodamine B) solution (0.4%w/v) were added and incubated in a dark place at room temperature for 10 min. Plates were washed three times with 1% acetic acid and allowed to air-dry overnight. Finally, 150 µL of Tris (10 mM) was added to dissolve the protein-bound SRB stain, and the absorbance was measured at 540 nm using a BMGLABTECH®-FLUO star Omega microplate reader (Ortenberg, Germany).

2.8 Antimicrobial activity of the produced ZnS-NPs

The antimicrobial activity of chemically and biosynthesized ZnS-NPs were investigated in vitro using disc diffusion assay against different Gram-positive (*Bacillus subtilis, Staphylococcus aureus*), Gram-negative bacteria (*Escherichia coli, Klebsiella pneumonia, Acinetobacter baumannii*), and *C.albicans* yeast. Stock inoculum suspensions of the strains were freshly prepared in 5 mL of sterile saline (0.9% NaCl w/v), from 24 h cultures grown on nutrient broth and Wickerham media for bacteria and yeast, at 37 and 28 °C, respectively. The optical density of the microbial growth was adjusted to achieve turbidity equivalent to 0.5 McFarland standard, ~1×10^8 CFU/mL for bacteria and 1×10^6 for *Candida* (Andrews 2001). The microbial inoculum was spread on plates containing an appropriate agar medium. Sterile discs were saturated with 20 µL of ZnS-NPs (10 mg/mL). Discs saturated with the same concentration of bulk ZnS were used as control. The experiment was carried out in triplicate, all plates were incubated at 37 °C for 24–48 h, and the inhibition zone diameter was measured in millimeters (Mani et al. 2018).

2.9 Statistical analysis

Experiments were conducted in triplicate; the mean and standard deviations were calculated using Excel software (Microsoft office 2010). Data were expressed as the mean values ± SD (standard deviation). For the photodegradation activity, one-way ANOVA was used using SPSS software (Version 17), and Tukey tests at P value (≤ 0.01) were carried out to find significant differences between different treatments.

3 Results and discussion

ZnS-NPs were biosynthesized using two different biological aqueous extracts for the first time; these were *U. fasicata* aqueous extract (UfaqE) and kumquat (*C. Japonica*) aqueous peel extract (KaqPE) (Fig. 1). The marine environment has always been attractive to researchers, because of its diversity of living organisms that can be exploited to produce various compounds, such as therapeutic metabolites, antibiotics, and nanoparticles (Adel et al. 2021; Kumar et al. 2021). In this regard, *Ulva fasicata* (genus Ulva), a genus of green algae (family Ulvaceae), represents one of the natural marine sustainable resources that contain various bioactive compounds, commonly used in nutraceutical and pharmaceutical industries (Namvar et al. 2014). *U. fasciata* is a marine macroalga commonly known as the "sea lettuce". It grows in the seashore of Alexandria, Egypt, during summer. On the other hand, *Citrus Japonica* is a member of the *Citrus* genus belonging to Rutaceae; it has been cultivated in Japan, China, Southeast Asia, and recently in Egypt. It is commonly known in markets as kumquat, edible due to the presence of carotenoids, ascorbic acid, flavonoids, and essential oils (Al-Saman et al. 2019). The biomolecules of UfaqE and KaqPE were simply extracted by hot water as an eco-friendly solvent and used as bio-reductants and stabilizing agents to produce ZnS-NPs. The reaction mixture color was changed from colorless to white or yellowish-white during the addition of Na_2S solution due to the formation of ZnS-NPs (Fig. 2).

EDTA and biological extracts interact with Zn^{2+} ions in the solution. At the first stage of the reactions, when EDTA or biological extracts were introduced, most of the Zn^{2+} ions were reserved in a coordinated form of $[Zn(EDTA)_m]^{+2}$. The Zn^{+2} released from the kinetic decomposition of $[Zn(EDTA)_m]^{+2}$ reacts with S^{-2} ions of Na_2S to produce ZnS-NPs capped with either EDTA or biomolecules (Eqs. 1–3). Such capping prevents NPs agglomeration and controls their shape and morphology as depicted by TEM analysis (Singh et al. 2021).

$$ZnSO_4 + m\,(EDTA) \xrightarrow{\text{Stirring 30 min}} \underset{\text{Coordinated form}}{\left\{Zn(EDTA)_m\right\}^{+2}} + \left(SO_4\right)^{-2} \quad (1)$$

$$\left\{Zn(EDTA)_m\right\}^{+2} \rightarrow Zn^{+2} + m(EDTA) \quad (2)$$

$$Zn^{+2} + Na_2S + m(EDTA) \rightarrow \underset{\text{Capped NPs}}{\{ZnS.EDTA\}} + 2Na^{+} \quad (3)$$

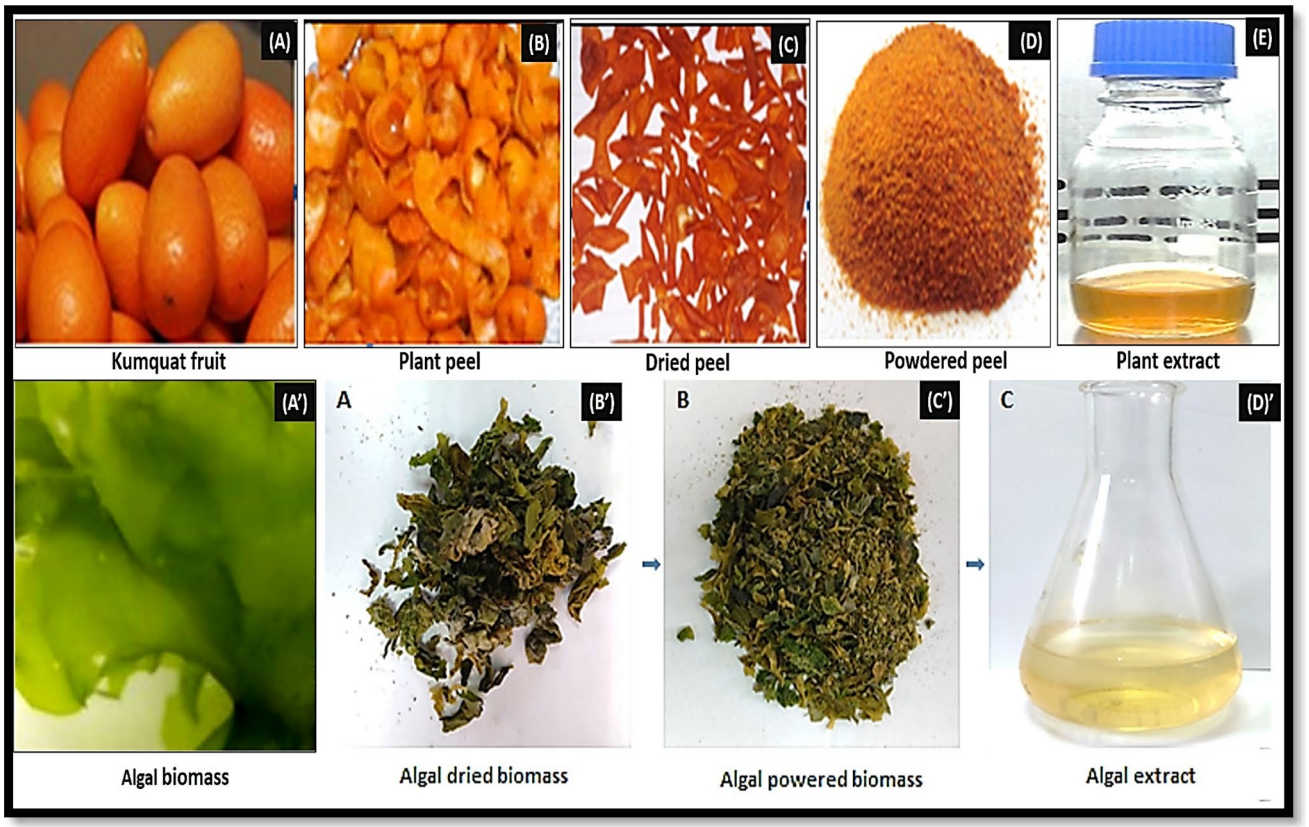

Fig. 1 Preparation of kumquat peels (**A**, **B**, **C**, **D**, **E**) and *Ulva fasciata* algal (**A'**, **B'**, **C'**, **D'**) extracts

3.1 Characterization of the produced ZnS-NPs

3.1.1 UV–Vis spectroscopy

UV–Vis spectroscopy is a very helpful method to identify the optical properties of nanomaterials (Kannan et al. 2020). Figure 2 shows two characterized sharp absorption peaks at 260 nm that correspond to the biosynthesized plant ZnS-NPs and algal ZnS-NPs, as compared with the absorption peak at 200 nm for the chemically synthesized ZnS-NPs. Furthermore, the algal ZnS-NPs have a maximum absorption peak, followed by the plant ZnS-NPs. Generally, maximum absorption wavelength (λmax) is reduced by reducing the NPs size as a result of quantum confinements of the photogenerated electron–hole carriers (Kannan et al. 2020). The band edge was shifted toward the longer wavelength side at 260 nm for the biosynthesized ZnS-NPs (Fig. 2). This shift in the absorption edge indicates the reduction in the band-gap energy of the biosynthesized ZnS-NPs (Kannan et al. 2020). The band-gap energy of chemically and biosynthesized ZnS-NPs was calculated to be 5.63 and 4.76 eV, respectively, which is greater than that of ZnS macromolecules (3.77 eV). The wide band-gap energy of the ZnS-NPs semiconductor is ideal for the photocatalytic activity due to the rapid generation of electron–hole pair by photoexcitation (Kannan et al. 2020). Therefore, the biosynthesized ZnS-NPs could be potentially used as active photocatalyst than ZnS macromolecules, under visible sunlight irradiation (Eyasu et al. 2013). The lower band-gap energy for the biosynthesized ZnS-NPs, as compared to chemically synthesized ones, is probably due to the presence of biomolecules in the biological extract used, stabilizing and capping the produced ZnS-NPs (Kannan et al. 2020).

3.2 X-ray diffraction (XRD)

Results obtained (Fig. 3) show the characteristic XRD peaks of the chemically synthesized ZnS-NPs at 28.4, 47.4, and 56.44° that correspond to the following crystalline planes of ZnS-NPs (111), (220), and (311), respectively, as reported by Wadhwani and Jain (2015). Similar XRD peaks for biosynthesized algal and plant Zn-NPs were exhibited at (28.58, 32.86, 47.650, and 56.48°), and (28.74, 32.86, 47.770, and 56.52°) that corresponded to (111), (200), (220) and (311), respectively. The three diffraction patterns of the chemically and biosynthesized ZnS-NPs confirmed the formation of cubic Zn-blend phase (sphalerite) of ZnS-NPs according to the standard sample

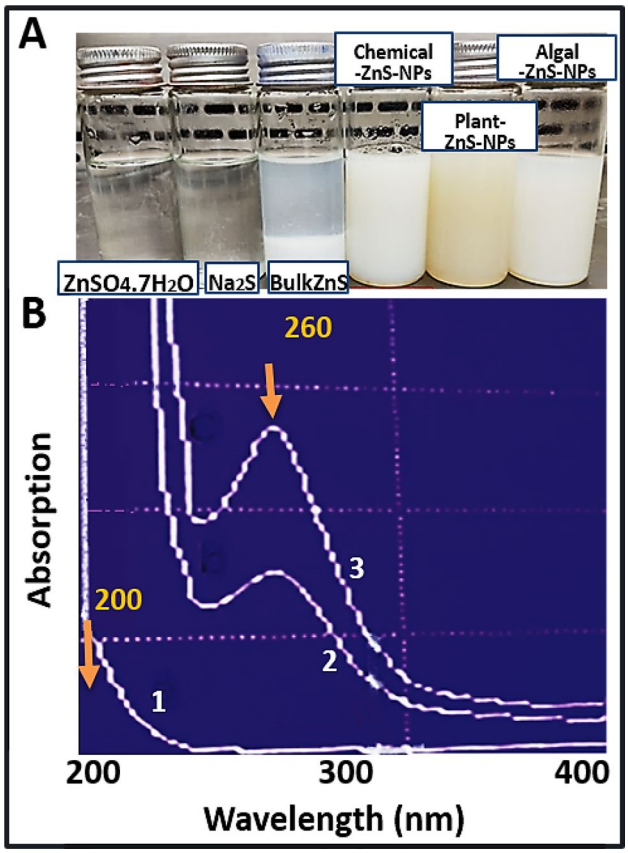

Fig. 2 The reaction mixture and formation of a white suspension of biosynthesized **A** plant, algal ZnS-NPs, and chemically synthesized ZnS-NPs; **B** UV–Vis spectroscopy of chemically synthesized ZnS-NPs, (1) biosynthesized plant ZnS-NPs (2) and algal ZnS-NPs (3)

published by the Joint Committee on Powder Diffraction Standards (JCPDS. no 05-0566) (Fig. 3). The broadness of the XRD peaks reveals the nanometric crystallite particle size of ZnS-NPs, and its higher sharpness indicates that NPs were highly crystalline. The diameter of ZnS-NPs has been estimated using Debye–Scherrer formula (Kannan et al. 2020):

$$D = 0.9\lambda/\beta \mathrm{Cos}\theta,$$

where ***D*** is the crystallite size, 0.9 is the constant shape factor, λ is the wavelength of X-rays (1.5405 Å) that represents the wavelength of incident beam CuKa1, β is a full-width half maximum of the peak (FWHM), and Θ is the diffraction angle in radian. According to the equation, the average size of the algal and plant ZnS nanocrystallites was calculated as 5.6 and 9.2 nm, respectively, as compared with the chemically synthesized ones having average diameter of 3.2 nm. Similarly, Ravikumar et al. (2021) reported that the cubic ZnS-blend (sphalerite) structure of the biosynthesized ZnS-NPs using *Costus speciosus* plant extract matched the standard card (JCPDS NO. 05–0566).

3.3 Transmission electron microscope (TEM)

TEM micrographs (Fig. 4) of chemically and biologically prepared NPs showed polydispersed NPs. Chemical ZnS-NPs were small, spherically shaped, with average diameter of 8–24 nm. Algal ZnS-NPs were spherically shaped, with average diameter that ranged 7–26 nm, while plant ZnS-NPs were cubic and polygonal, with particle size that ranged 24–31 nm. The variation in size and morphology between chemically and biosynthesized ZnS-NPs highly depends on the capping and stabilizing agents used in the synthesis process (Mani et al. 2018).

3.4 Energy-dispersive absorption X-ray spectroscopy (EDAX)

The elemental configuration and purity of the NPs were determined by EDAX (Fig. 5). The EDAX pattern shows strong signals in the regions of Zn and S that confirm the presence of ZnS. Other signals from C and O atoms were also recorded, where C and O were attributed to elements present within the used biological extracts. The average atomic ratio of Zn/S, calculated from the quantification of the peaks (excluded C and O), were 56.31:43.69, 65.8:38.3, and 52.6:43.3 for chemical, plant, and algal ZnS-NPs, respectively. Similarly, Kannan et al. (2020) reported that the main elements in chemically synthesized ZnS-NPs were Zn (50.38%) and S (49.62%), while the biosynthesized ZnS-NPs showed Zn (49.54%) and S (48.36%) elements along with O (1.10%) and C (1.00%) elements, which were present in the plant extract of *Tridax procumbens* used for biosynthesis. The deviation of atomic ratio of Zn:S to the expected 1:1 could also be attributed to the excessive Zn ions absorbed on the surface of NPs. Results (Fig. 5) revealed that the surface of all produced NPs were rich in Zn due to the absorption of Zn ions on its surface, which was far larger than that of the bulk materials.

3.5 Fourier transform infrared spectroscopy (FTIR)

FTIR analysis (Fig. 6) showed peaks at 627 cm^{-1}, 615 cm^{-1}, and 617 cm^{-1} for chemical, plant, and algal ZnS-NPs, respectively, due to the stretching vibration of Zn and S bonds (Mourdikoudis et al. 2018). A strong and sharp peak appeared for plant and algal ZnS-NPs at 1447 cm^{-1} and 145 cm^{-1} due to ammonium ions (Mourdikoudis et al. 2018). Several peaks were observed for chemical, plant, and algal ZnS-NPs from 1400 cm^{-1} to 1732 cm^{-1} due to C = O carboxylic stretching. Strong broad peaks appeared at 3430 cm^{-1}, 3413 cm^{-1}, and 3430 cm^{-1} for chemical, plant, and algal ZnS-NPs, respectively, due to the N–H amine groups, and others appeared

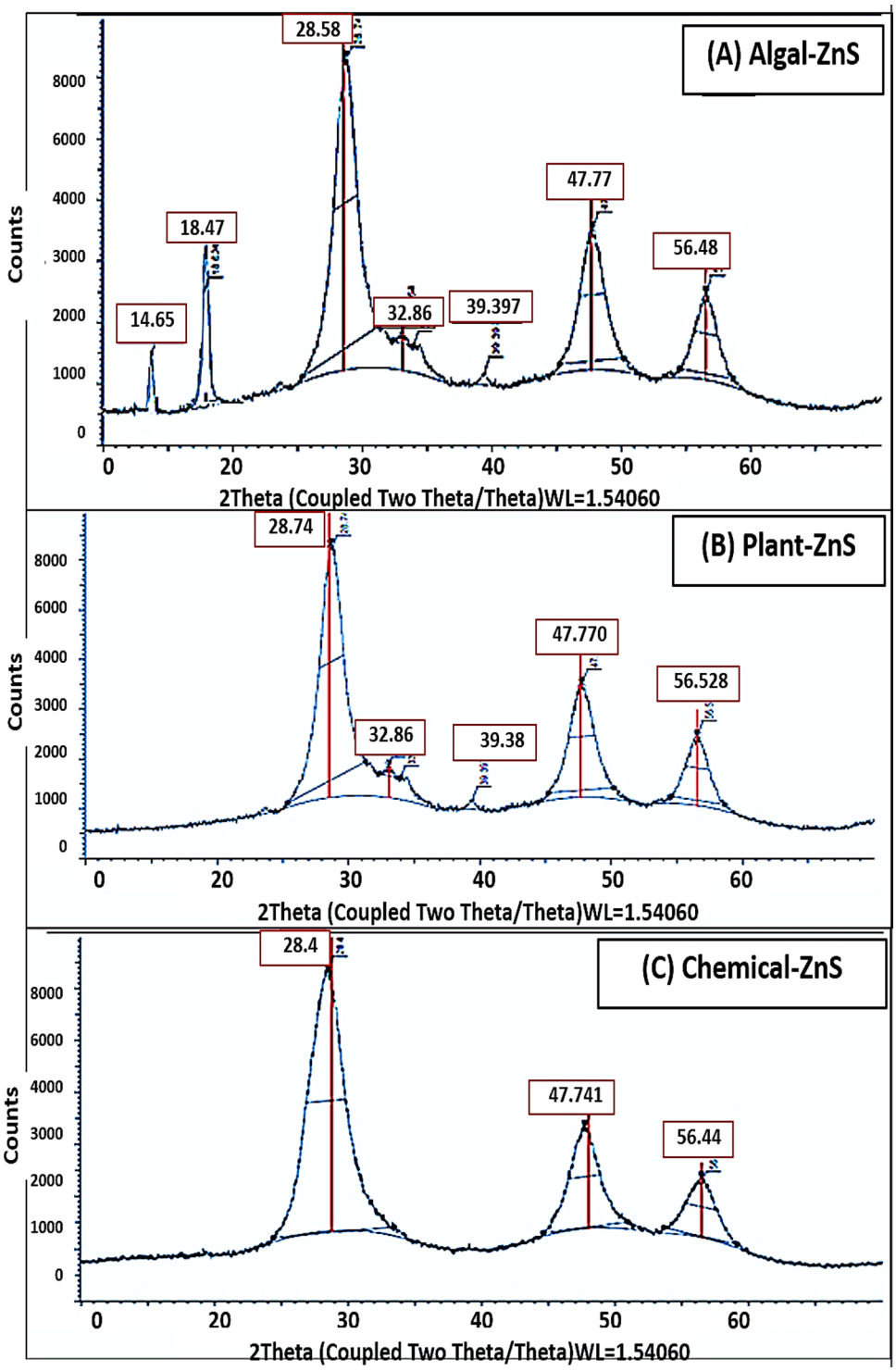

Fig. 3 XRD of ZnS-NPs synthesized by algae (**A**), plant (**B**), and chemically (**C**)

from 3772 to 3991 cm^{-1} due to the –OH hydroxyl groups (Fig. 6). The N–H amines and –OH hydroxyl peaks were reported for the stabilization of NPs (Kannan et al. 2020). Unlike the chemical ZnS-NPs, the biosynthesized plant and algal ZnS-NPs had several absorbance bands, due to the presence of protein biomolecules that commonly act as stabilizing and reducing agents for the produced ZnS-NPs.

3.6 Photodegradation of CV, SF, and industrial wastewater

Dye effluents discharged into water bodies represent one of the major types of pollutants released from textile industry and other industrial processes (Rafiq et al. 2021). These dyes are very toxic and carcinogenic. Therefore, treatment of

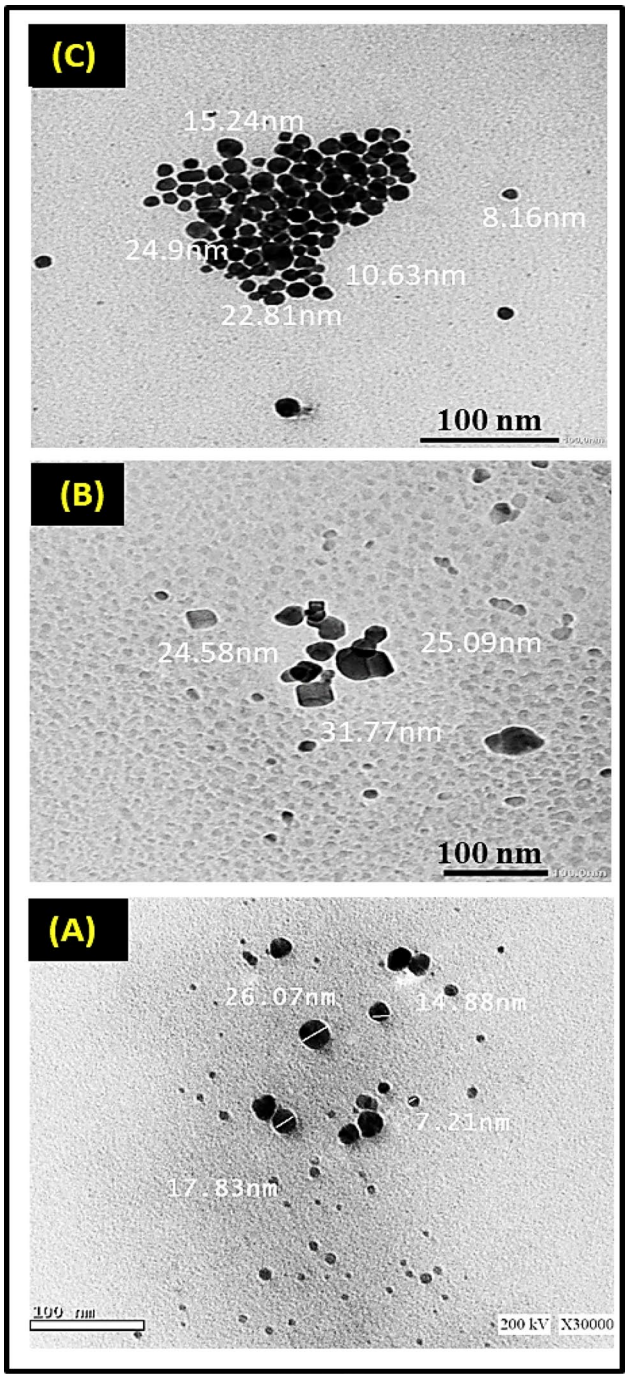

Fig. 4 TEM micrograph of algal ZnS-NPs (**A**), plant ZnS-NPs (**B**), and chemically synthesized ZnS-NPs (**C**)

wastewater is necessary to avoid their harmful effect on the environment and human health. In this respect, the photocatalytic degradation of dyes was recommended because of its excellent efficiency and performance (Eyasu et al. 2013; Rafiq et al. 2021). CV and SF are of the most widely used dyes in various fields. CV, known as gentian violet or Tris 4-(dimethylamino) phenyl) methylium chloride, is used in medical and scientific applications, in textile and paper dyes, inks, and coloring various products (Maley and Arbiser, 2013). While SF is the azonium compound of symmetrical 2,8-dimethyl-3,7-diamino-phenazine, SF-O dye is a textile staining dye for cotton, fibers, silk, wool, and leather (Oda et al. 2016).

In the present study, the photocatalytic activity of chemically and biosynthesized ZnS-NPs was evaluated toward CV and SF dyes, as well as industrial wastewater contaminated by dye residues released from the textile industry. Results revealed that the degradation efficiency of CV, SF, and wastewater was only 9.5, 10 and 12%, respectively, using no catalyst under sunlight irradiation, and was stable after 120 min. However, the photodegradation efficiency was significantly increased using 10 mg/100 mL of chemical, plant, or algal ZnS-NPs as the photocatalyst (Fig. 7). Prominent peaks at λ_{585} and λ_{518} nm were decreased gradually with the increase of exposure time to sunlight irradiation for CV and SF, respectively, which implies that these dyes had been degraded. The degradation efficiency (Fig. 7) for CV using chemical, plant, and algal ZnS-NPs were 89, 82.5 and 98.12%, respectively, after 90 min irradiation time, after which CV was completely degraded. In addition, the degradation efficiency of SF using chemical, plant, and algal ZnS-NPs (Fig. 8) were 90, 84 and 95.9%, respectively, after 180 min.

Furthermore, the photodegradation of industrial wastewater released from textile industry (Alrobaeia Textile Factory, 6th Industrial region, Sadat city, Egypt) was evaluated using chemical, plant, or algal ZnS-NPs as the photocatalyst. This industrial wastewater consists of five different dye residues (reactive dye 76% sulfur dye, indigo dye, coating dye, and others). Results obtained (Fig. 9) show maximum absorption peak at λ_{620} nm, which was diminished in the presence of ZnS-NPs as the photocatalyst. The degradation efficiency of chemical, plant, and algal ZnS-NPs was observed to be 88.9, 82 and 96.8%, respectively, after 160 min irradiation time (Fig. 9). The performance of a photocatalyst relies primarily on its capability to absorb electromagnetic radiation to produce electron–hole pairs, responsible for photocatalysis through oxidation–reduction reactions (Kannan et al. 2020). The obtained results revealed that algal ZnS-NPs have the highest significant degradation efficiency as compared to other Zn-NPs. The biomolecules present in the biological extracts act as capping agents and increase the catalytic activity than chemically synthesized nanosized ZnS by the reduction in electron–hole recombination (Kannan et al. 2020). These biomolecules may influence ZnS crystal growth with high surface area to its volume ratio, which increases the generation of electron–hole pairs under visible light irradiation. Also, the increase in band-gap energy of biosynthesized ZnS-NPs increases its oxidative capability when exposed to

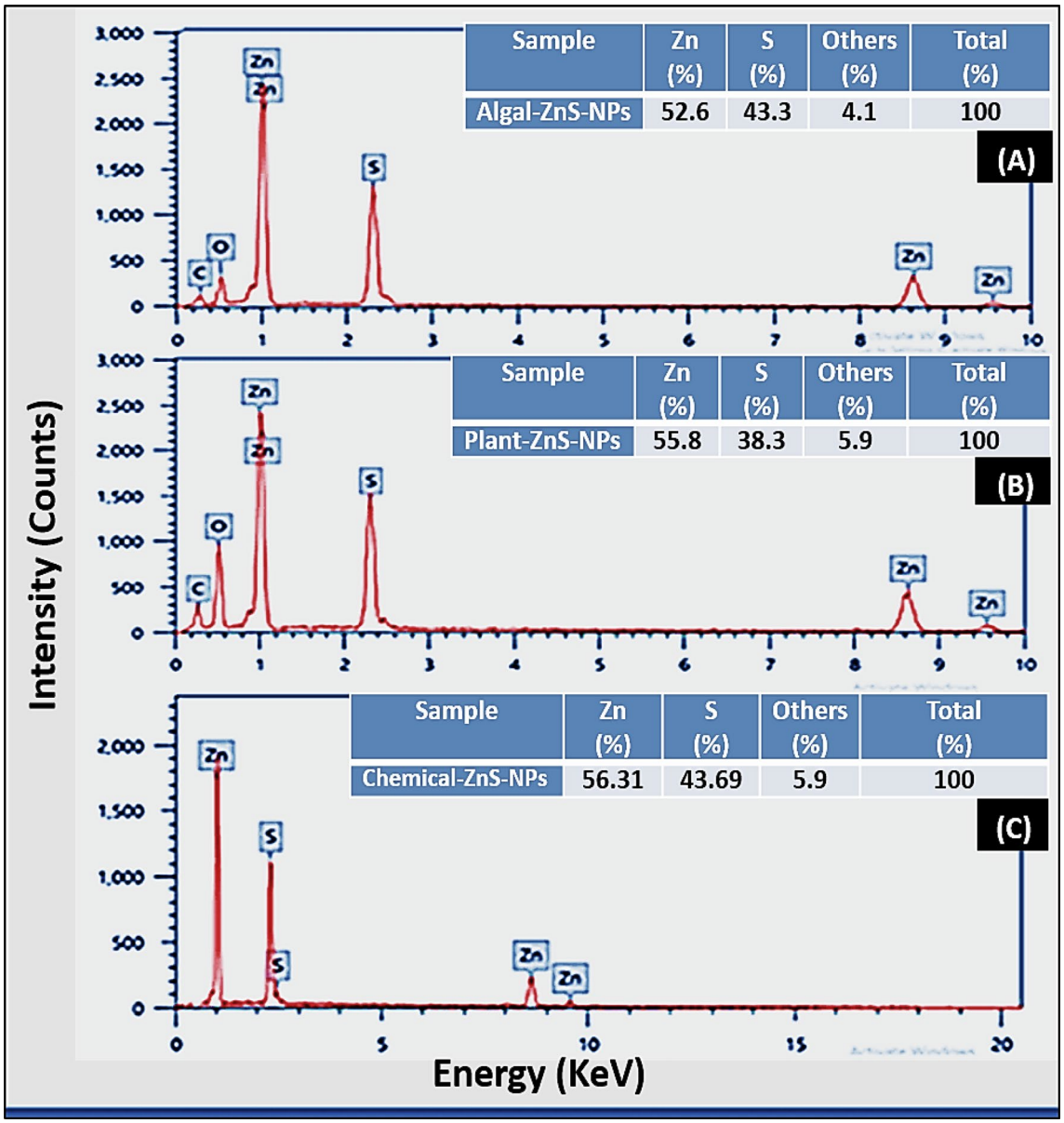

Fig. 5 EDAX analysis of biosynthesized plant, algal ZnS-NPs (**A**, **B**) and chemically synthesized ZnS-NPs (**C**) showing elemental composition with percentage (%)

sunlight irradiation (Ajibade et al. 2020). Similarly, Kannan et al. (2020) reported that biosynthesized ZnS-NPs were used as efficient biocatalysts for the degradation of methylene blue under visible light irradiation for 180 min, with degradation efficiency of 74 and 99% for chemical nanosized ZnS and biosynthesized ZnS-NPs, respectively. In addition, Ravikumar et al. (2021) fabricated ZnO-NPs and ZnS-NPs using *Costus speciosus* leaf extract and revealed their complete photocatalytic degradation of Reactive Red-120 dye within 180 min.

3.7 Photodegradation mechanism and recyclability

ZnS is a metal sulfide belonging to semiconductors that can faster generate electron–hole pairs; therefore, they are extensively used in photoelectricity, catalysis, photosensors, etc. (Sirajudheen et al. 2021). In semiconductor materials, free charge carriers are electrons (e^-) and electron–holes (h^+). During irradiation, the photoexcitation of ZnS results in the movement of (e^-) from the valence band (VB) to the conduction band (CB), leaving a hole

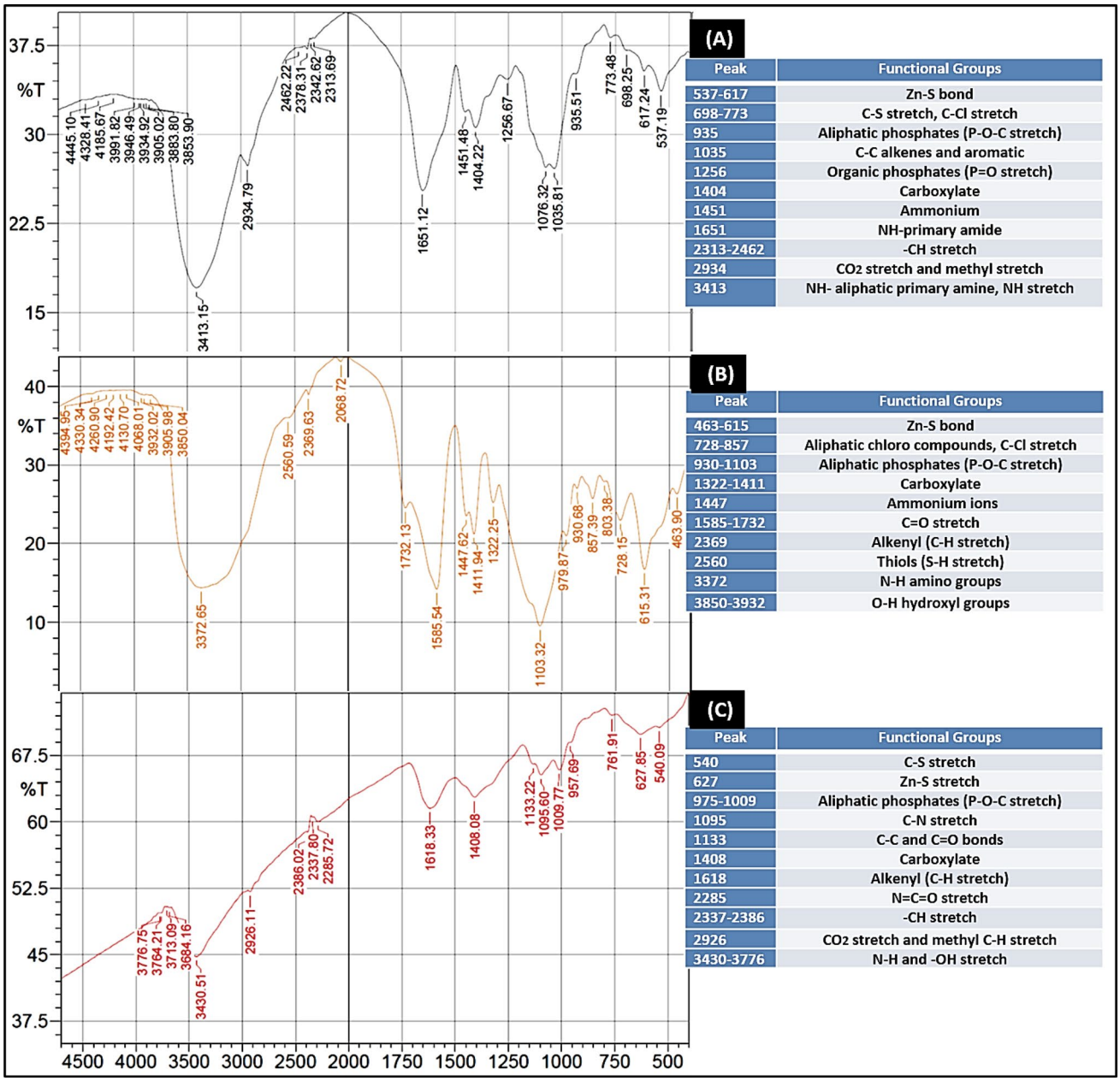

Fig. 6 FTIR spectroscopy of algal ZnS-NPs (**A**), plant ZnS-NPs (**B**), and chemical ZnS-NPs (**C**)

(h^+); these electron–holes (h^+) can move from an atom to another in semiconductors (Sirajudheen et al. 2021). ZnS-NPs as a catalyst adsorb the dye onto their surface when exposed to visible light, which causes photoexcitation of electrons and generation of electron–hole pairs. These photogenerated electrons in the conduction band of ZnS interact with water and/or atmospheric oxygen (O^{-2}) forming highly reactive radicals ($O_2^{\blacksquare}$) adsorbed on the ZnS surface. The holes created in the valence band of ZnS also interact with H_2O molecules and/or (OH^-) groups to give highly reactive hydroxyl radicals ($OH^{\blacksquare}$), which are very powerful oxidizing agents (Sirajudheen et al. 2021). These highly reactive hydroxyl radicals and superoxide radicals are responsible for direct and indirect oxidation of the dye adsorbed on the nanosized ZnS, leading to its degradation as proposed in the following equations (Sirajudheen et al. 2021):

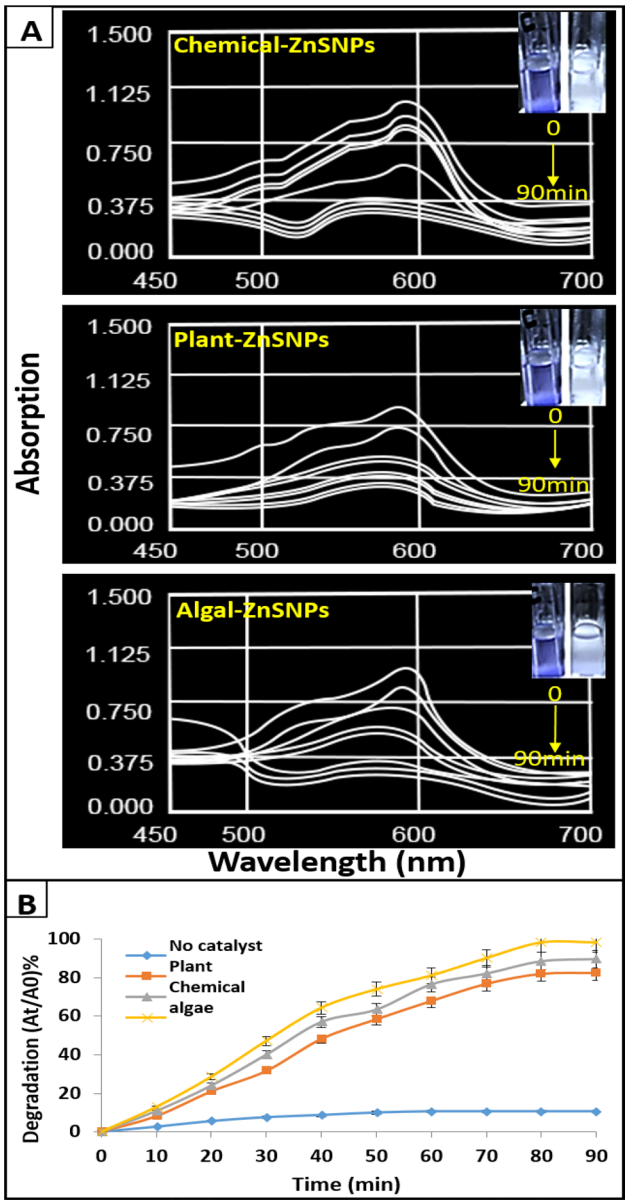

Fig. 7 UV–Vis spectra for photocatalytic degradation of crystal violet dye **A** and its photodegradation efficiency **B** using chemical, plant, and algal ZnS-NPs

$$\text{Sunlight} \quad Nanosized\ ZnS + h\nu \rightarrow nanosized\ ZnS\ (e^-_{CB} + h^+_{VB})$$

$$ZnS(h^+_{VB}) + H_2O \rightarrow ZnS + OH^- + H^+$$

$$ZnS(h^+_{VB}) + OH^- \rightarrow ZnS + OH^{\cdot}$$

$$ZnS(he^-_{CB}) + O_2 + H \rightarrow ZnS + HO^{\cdot}_2 + H^+$$

$$ZnS(he^+_{VB}) + O_2 \rightarrow ZnS + O^{-\cdot}_2$$

$$(O^{-\cdot}_2) + H^+ \rightarrow HO^{\cdot}_2$$

$$e^- + H_2O_2 \rightarrow OH^- + OH^{\cdot}$$

$$OH^{\cdot} + ZnS(h^+_{VB}) + O_2 + Dyes \rightarrow CO_2 + HO_2 + Other\ products$$

$$(Photodegradation\ of\ Dyes)$$

The degradation process relies on the particle size, surface area, and the morphology of the nanocrystals, which could improve the properties of the photogenerated electron–hole pairs (Sirajudheen et al. 2021). Also, the transportation time of electron–hole from the crystal interface to its surface at nanoscale is shorter than that in macroscale, which helps to increase the charge migration rate to its surface, and thus the photocatalytic process (Beydoun et al. 1999; Sirajudheen et al. 2021). In addition, the stability test is one of the important parameters for practical application of photocatalyst. After three cycles, the prepared ZnS-NPs showed excellent reusability with stability (Fig. 10). Recently, Sirajudheen et al. (2021) produced a ZnS/chitosan matrix and reported its photocatalytic activity of 87.3 and 91.5% toward methylene blue, and malachite green dyes, respectively, after 60 min of visible light irradiation and was reusable up to five cycles.

3.8 Antimicrobial activity

The antimicrobial activity of chemical, plant, and algal ZnS-NPs was examined against some pathogenic Gram-positive, Gram-negative bacteria, and yeast strains (Table 1). Biosynthesized ZnS-NPs showed the highest antimicrobial effect as compared to chemically synthesized ZnS-NPs against all tested microbial strains. The higher antimicrobial activity belongs to algal ZnS-NPs that showed maximum inhibition zone of 22 ± 0.3, 20 ± 0.3, 19 ± 0.1, 27 ± 0.3, 26 ± 0.3, and 20 ± 0.1 mm against *B. subtilis, S. aureus, A. baumannii, E. coli, K. pneumonia,* and *C. albicans,* respectively. Similar antimicrobial effect was observed by the plant ZnS-NPs with no significant difference (Table 1). Results reveal that the Gram-negative *E. coli* was the most sensitive strain to ZnS-NPs with maximum inhibition zone of 27 ± 0.5, 25 ± 0.3, and 19 ± 0.1 mm for algal, plant, and chemically synthesized ZnS-NPs, respectively. The results obtained are probably

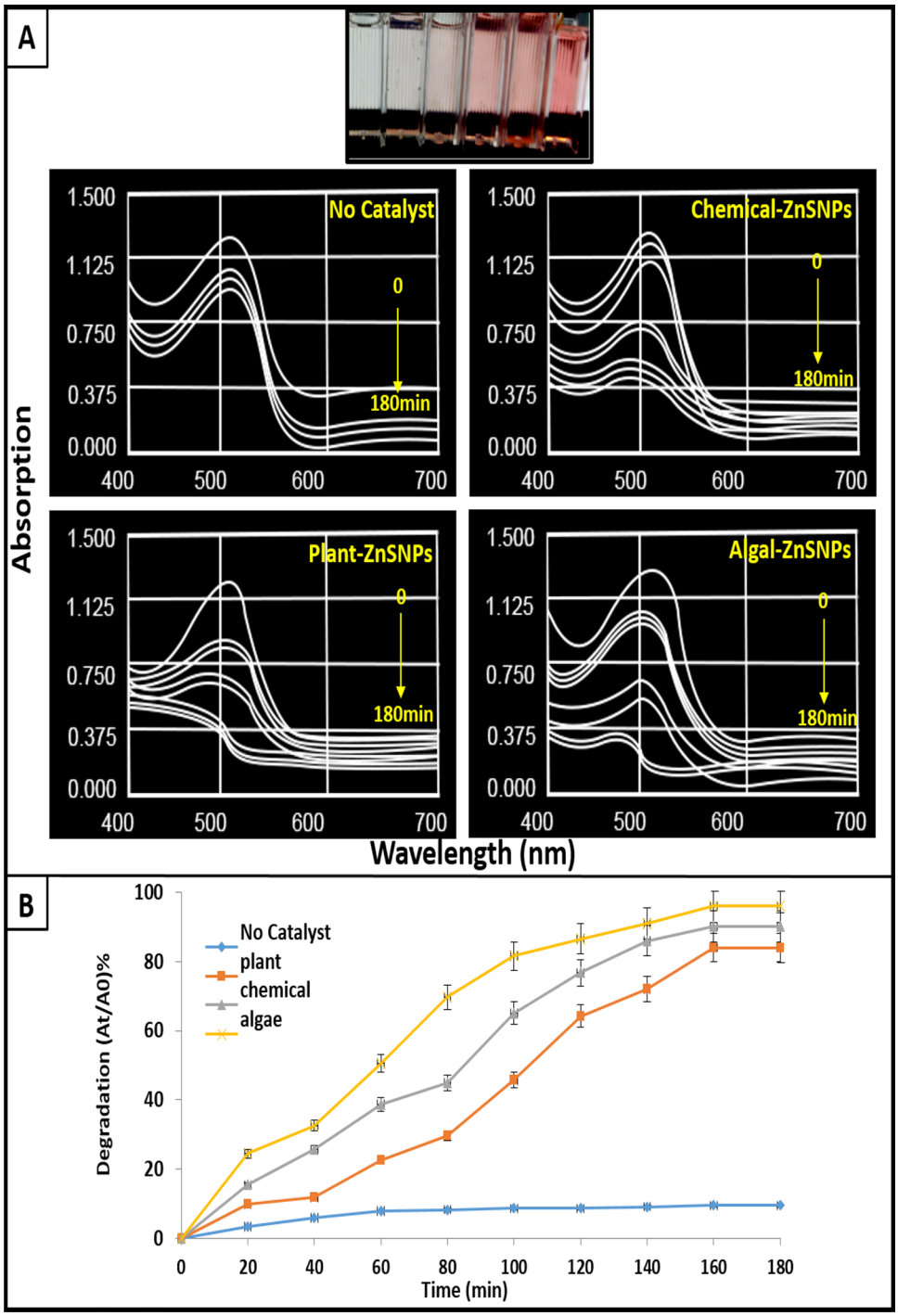

Fig. 8 UV–Vis spectra for photocatalytic degradation of safranin dye **A**, and its photodegradation efficiency **B**, using chemical, plant, and algal ZnS-NPs

due to the difference in microbial cell wall structure (Mani et al. 2018). The cell wall of Gram-negative bacteria has double thin layer of lipopolysaccharide, followed by a very thin peptidoglycan layer, which facilitate the rapid penetration of ZnS-NPs into the cell, causing its damage (Mani et al. 2018). Plant and algal extracts also contain secondary metabolites, such as enzymes, phenols, flavonoids, and alkaloids, which act as capping agents for biosynthesized ZnS-NPs. These biomolecules can react with the carboxyl, sulfhydryl groups, and the amide-phosphate in microbial cell membrane, causing its damage (Ham and Jang, 2018). Furthermore, reactive oxygen spp. generated during the interaction of ZnS-NPs with water and/or oxygen molecules when exposed to light can break down the lipopolysaccharides and the peptidoglycan layer, leading to peroxidation of the lipid membrane and oxidation of proteins, thus causing microbial

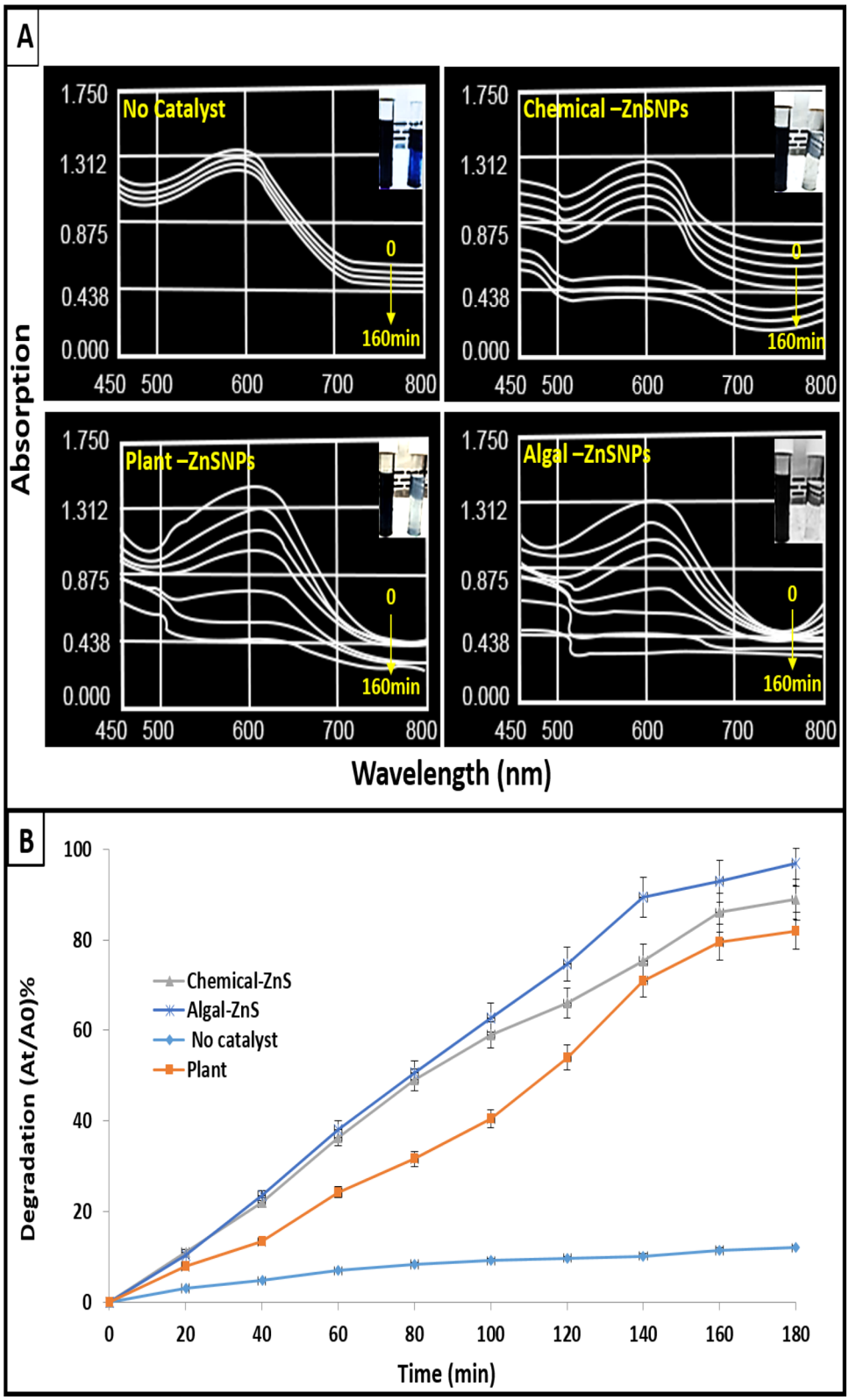

Fig. 9 UV–Vis spectra for photocatalytic degradation of textile industrial wastewater **A**, and its photodegradation efficiency **B**, using chemical, plant, and algal ZnS-NPs

death (Kannan et al. 2020). Similarly, Mani et al. (2018) prepared ZnS-NPs using the extracts of *Tridax procumbens* and *Syzygium aromaticum* and reported the highest antimicrobial effect with inhibition zone of 29 mm against *C. albicans*, followed by *E. coli* (24 mm), *P. aeruginosa* (23 mm), *S. aureus* (23 mm), and *B. subtilis* (22 mm).

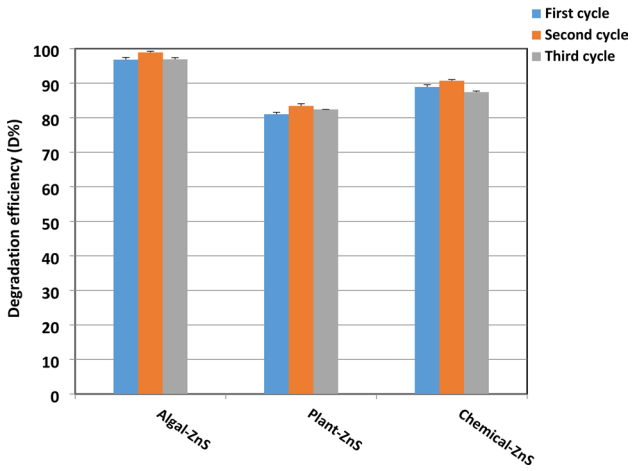

Fig. 10 Recyclability and reusability of chemically and biosynthesized ZnS-NPs photocatalyst for textile industrial wastewater treatment

bioactive molecules present in the biological source used for biogenic synthesis and capping of ZnS-NPs, which influenced its properties (Paknejadi et al. 2018; Roy et al. 2019), and verified by FTIR as O–H, N–H, C–H, C–O–C, and C–NH_2. The potential cytotoxicity of NPs depends on the routes of administration and NPs characteristics, such as size, shape, concentration, and time exposure, as well as the capping agent used for NPs stabilization (Niska et al. 2016; Tayel et al. 2017; Paknejadi et al. 2018). In this regard, Hazra et al. (2013) biosynthesized ZnS-NPs using rhamnolipids biosurfactant extracted from *P. aeruginosa* BS01 as capping/stabilizing agent and tested the cytotoxic effect in vitro against rat hepatocyte cell lines. Hazra et al. (2013) reported 25 µg/mL IC_{50} and 70 µg/mL for ZnS-NPs capped by SDS and ZnS-NPs capped by rhamnolipids, respectively, which indicates that the type of capping highly affects the cytotoxicity of NPs. Likewise, our results (Fig. 11) revealed that algal and plant ZnS-NPs

Table 1 Antimicrobial activity of chemical, algal and plant ZnS-NPs against different pathogenic strains of Gram-positive and Gram-negative bacteria, and yeast expressed as mean inhibition zone diameter of three replicates in mm ± SD

ZnS-NPs	Zone of inhibition (mm)					
	Fungi	Gram-negative			Gram-positive	
	C. albicans	*K. pneumonia*	*E. coli*	*A. baumannii*	*S. aureus*	*B. subtilis*
Algal ZnS NPs	20 ± 0.3	26 ± 0.3	27 ± 0.5	19 ± 0.1	20 ± 0.0	22 ± 0.3
Plant ZnS NPs	18 ± 0.1	24 ± 0.3	25 ± 0.1	18 ± 0.5	18 ± 0.3	20 ± 0.3
Chemical ZnS-NPs	5 ± 0.3	17 ± 0.3	19 ± 0.3	5 ± 0.3	14 ± 0.3	16 ± 0.1
Bulk ZnS	0 ± 0	0 ± 0	0 ± 0	0 ± 0	0 ± 0	0 ± 0

NPs: nanoparticles

3.9 Cytotoxicity of the produced ZnS-NPs

For safe applications of the produced ZnS-NPs, its cytotoxicity was evaluated on human skin fibroblast (HSF) normal cell lines using SRB assay. The SRB assay is an efficient and highly cost-effective technique to examine drug toxicity against various types of tumorous and non-tumorous cell lines (Vichai and Kirtikara, 2006). The algal ZnS-NPs and plant ZnS-NPs exhibited relatively less cytotoxicity to HSF normal cell lines with $IC_{50} < 300$ µg/mL as compared with chemically synthesized ZnS-NPs. Treatment with different concentrations of biologically synthesized ZnS-NPs did not show visible cytotoxicity to HSF cell lines (Fig. 11). The IC_{50} of chemically synthesized ZnS-NPs was found to be 88 µg/mL, which was less than the IC_{50} of biosynthesized ZnS-NPs, > 300 µg/mL. Therefore, chemically synthesized ZnS-NPs induced toxic effect on cells causing their death at lower concentration than the biosynthesized ZnS-NPs and at the same tested concentrations (Fig. 11). The lower toxicity of biosynthesized ZnS-NPs is probably due to the

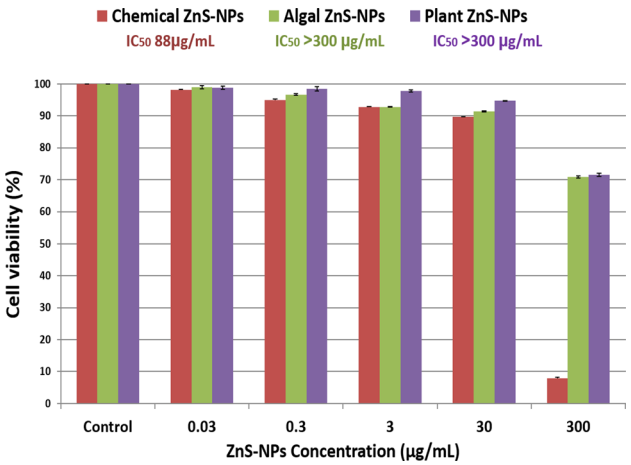

Fig. 11 Cytotoxic effect of chemically synthesized ZnS-NPs, algal ZnS-NPs, and plant Zns-NPs, tested against human skin fibroblast (HSF) regular cell lines using SRB assay with IC_{50} calculated in µg/mL

capped by biomolecules from UfaqE and KPaqE have less cytotoxic effect ($IC_{50} < 300$ µg/mL) than that capped by EDTA (IC_{50} of 88 µg/mL), which probably makes it safer for water treatment.

4 Conclusion

A simple biosynthesis approach for efficient water treatment was described using a cost-effective and eco-friendly technique. IC_{50} of biosynthesized ZnS-NPs on HSF cell lines was > 300 µg/mL being safer than chemically synthesized ones. Biosynthesized ZnS-NPs exhibited excellent photocatalytic activity toward industrial wastewater contaminated with textile dyes and two organic dyes (CV and SF), with significant degradation efficiency and recyclability up to three cycles, and thus can be used in many industrial applications. Biosynthesized ZnS-NPs exhibited the highest antimicrobial activity against different pathogenic strains, as compared to chemically synthesized ones. The smaller-sized algal ZnS-NPs have lower recombination rate of electron–hole pairs and larger reactive surface area for the adsorption of dye molecules, leading to better photocatalytic performance. The observed enhancement in the antimicrobial and photodegradation activities is probably due to the biomolecules present in biological extracts, which improved the properties of biosynthesized ZnS-NPs, as compared to chemically synthesized ones. FTIR verified that biosynthesized plant and algal ZnS-NPs have several absorbance bands, due to the presence of different biomolecules that commonly act as stabilizing and capping agents for the produced NPs, which did not appear in chemical ZnS-NPs capped with EDTA. These biomolecules have given NPs more stability in photocatalytic degradation and higher antimicrobial activity, with lower cytotoxicity as compared to chemically synthesized ones, which probably enhance their safe application. The overall results suggest using the novel biosynthesized ZnS-NPs as powerful safe bio-photocatalyst, with considerable antimicrobial activity for the treatment of water/wastewater containing dye through a simple and cost-effective approach.

Author contributions Conceptualization, writing, and editing: NS and RA. Laboratory work and data analysis: AE, NS and RA. All authors read and approved the manuscript. All Supplementary data are available upon request.

Funding Open access funding provided by The Science, Technology & Innovation Funding Authority (STDF) in cooperation with The Egyptian Knowledge Bank (EKB). This work was funded by the Academy of Scientific Research and Technology (ASRT), EGYPT for Green nano-preparation and applications at GEBRI, University of Sadat City, Egypt.

Declarations

Conflict of interest All authors declare that there are no financial/commercial conflicts of interest.

References

Adel A, El-Baz A, Shetaia Y, Sorour NM (2021) Biosynthesis of polyunsaturated fatty acids by two newly cold-adapted Egyptian marine yeast. 3 Biotech 11:1–15

Ahmed SO, Nasser AA, Abbas RN et al (2021) Production of bioconcrete with improved durability properties using Alkaliphilic Egyptian bacteria. 3B Iotech 11:1–15

Ajibade PA, Oluwalana AE, Sikakane BM et al (2020) Structural, photocatalytic and anticancer studies of hexadecylamine capped ZnS nanoparticles. Chem Phys Lett 755:137813

Alijani HQ, Pourseyedi S, Mahani MT et al (2019) Green synthesis of Zinc Sulfide (ZnS) nanoparticles using *Stevia rebaudiana Bertoni* and evaluation of its cytotoxic properties. J Mol Struct 1175:214–218

Al-Saman MA, Abdella A, Mazrou KE et al (2019) Antimicrobial and antioxidant activities of different extracts of the peel of Kumquat (*Citrus japonica Thunb*). J Food Meas Charact 13:3221–3229

Ambigadevi J, Kumar PS, Vo DV et al (2021) Recent developments in photocatalytic remediation of textile effluent using semiconductor based nanostructured catalyst: a review. J Environ Chem Eng 9:104881

Andrews JM (2001) Determination of minimum inhibitory concentrations. J Antimicrob Chemother 48:5–16

Beydoun D, Amal R, Low G et al (1999) Role of nanoparticles in photocatalysis. J Nanopart Res 1:439–458

Chan YY, Pang YL, Lim S et al (2021) Facile green synthesis of ZnO nanoparticles using natural-based materials: properties, mechanism, surface modification and application. J Environ Chem Eng 9:105417

Dhir R (2021) Synthesis, characterization and applications of Gadolinium doped ZnS nanoparticles as photocatalysts for the degradation of dyes (Malachite Green and Rhodamine B) and as antioxidants. Chem Phys Impact 3:100027

El-Baz AF, Sorour NM, Shetaia YM (2016) *Trichosporon jirovecii*–mediated synthesis of cadmium sulfide nanoparticles. J Basic Microbiol 56:520–530

Eyasu A, Yadav OP, Bachheti RK (2013) Photocatalytic degradation of methyl orange dye using Cr-doped ZnS nanoparticles under visible radiation. Int J Chem Tech Res 5:1452–1461

Ham S, Jang DJ (2018) Facile photohydroxylation of ZnS nanobelts for enhanced photocatalytic activity. J Environ Chem Eng 6:228–235

Hamouda RA, Yousuf WE, Mohammed AA et al (2020) Comparative study between zinc oxide nanoparticles synthesis by biogenic and wet chemical methods in vivo and in vitro against *Staphylococcus aureus*. Microb Pathog 147:104384

Hassan A, Sorour NM, El-Baz A et al (2019) Simple synthesis of bacterial cellulose/magnetite nanoparticles composite for the removal of antimony from aqueous solution. Int J Environ Sci Technol 16:1433–1448

Hazra C, Kundu D, Chaudhari A et al (2013) Biogenic synthesis, characterization, toxicity and photocatalysis of zinc sulfide nanoparticles using rhamnolipids from pseudomonas aeruginosa BS01 as capping and stabilizing agent. J Chem Technol Biotechnol 88:1039–1048

Kannan S, Subiramaniyam NP, Sathishkumar M (2020) A novel green synthesis approach for improved photocatalytic activity and antibacterial properties of zinc sulfide nanoparticles using plant extract of *Acalypha indica* and *Tridax procumbens*. J Mater Sci-Mater Electron 31:9846–9859

Kumar BR, Mathimani T, Sudhakar MP et al (2021) A state of the art review on the cultivation of algae for energy and other valuable products: application, challenges, and opportunities. Renew Sustain Energy Rev 138:110649

Maley AM, Arbiser JL (2013) Gentian violet: a 19th century drug re-emerges in the 21st century. Exp Dermatol 22:775–780

Mani SK, Saroja M, Venkatachalam M et al (2018) Antimicrobial activity and photocatalytic degradation properties of ZnS nanoparticles synthesized by using plant extracts. J Nanostructures 8:107–118

Mansur AA, Mansur HS, Ramanery FP et al (2014) "Green" colloidal ZnS quantum dots/chitosan nano-photocatalysts for advanced oxidation processes: study of the photodegradation of organic dye pollutants. Appl Catal B 158:269–279

Mourdikoudis S, Pallares RM, Thanh NT (2018) Characterization techniques for nanoparticles: comparison and complementarity upon studying nanoparticle properties. Nanoscale 10:12871–12934

Namvar F, Baharara J, Mahdi AA (2014) Antioxidant and anticancer activities of selected Persian Gulf algae. Indian J Clin Biochem 29:13–20

Niska K, Knap N, Kędzia A et al (2016) Capping agent-dependent toxicity and antimicrobial activity of silver nanoparticles: an in vitro study. Concerns about potential application in dental practice. Int J Med Sci 13:772

Oda AM, Khuder H, Hashim R et al (2016) Photocatalytic degradation of safranin O by ZnO-Ag loaded on cotton fabric. Res J Pharm, Biol Chem Sci 7:2915–2924

Paknejadi M, Bayat M, Salimi M et al (2018) Concentration-and time-dependent cytotoxicity of silver nanoparticles on normal human skin fibroblast cell line. Iran Red Crescent Med J 20:10

Qamar SA, Asgher M, Khalid N et al (2019) Nanobiotechnology in health sciences: current applications and future perspectives. Biocatal Agric Biotechnol 22:101388

Rafiq A, Ikram M, Ali S et al (2021) Photocatalytic degradation of dyes using semiconductor photocatalysts to clean industrial water pollution. J Ind Eng Chem 97:111–128

Rajabi HR, Sajadiasl F, Karimi H et al (2020) Green synthesis of zinc sulfide nano photocatalysts using aqueous extract of *Ficus Johannis* plant for efficient photodegradation of some pollutants. J Market Res 9:15638–15647

Rao MD, Pennathur G (2016) Facile bio-inspired synthesis of zinc sulfide nanoparticles using Chlamydomonas reinhardtii cell-free extract: optimization, characterization and optical properties. Green Process Synth 5:379–388

Ravikumar S, Pandiyan V, Alam M et al (2021) *Costus speciosus* Koen leaf extract assisted cs-znx (X=O or S) nanomaterials: synthesis, characterization and photocatalytic degradation of RR120 dye under UV and direct sunlight. J Mol Struct 1225:129176

Reenaa M, Menon AS (2017) Synthesis of silver nanoparticles from different citrus fruit peel extracts and a comparative analysis on its antibacterial activity. Int J Curr Microbiol App Sci 6:2358–2365

Roy A, Bulut O, Some S, Mandal AK, Yilmaz MD (2019) Green synthesis of silver nanoparticles: biomolecule-nanoparticle organizations are targeting antimicrobial activity. RSC Adv 9:2673–2702

Sadovnikov SI (2019) Synthesis, properties, and applications of semiconductor nanostructured zinc sulfide. Russ Chem Rev 88:571

Sirajudheen P, Kasim VR, Nabeena CP et al (2021) Tunable photocatalytic oxidation response of ZnS tethered chitosan-polyaniline composite for the removal of organic pollutants: a mechanistic perspective. Mater Today: Proc 47:2553–2559

Singh M, Vaya D, Kumar R, Das B (2021) Role of EDTA capped cobalt oxide nanomaterial in photocatalytic degradation of dyes. J Serb Chem Soc 86:327–340

Skehan P, Storeng R, Scudiero D et al (1990) New colorimetric cytotoxicity assay for anticancer-drug screening. JNCI: J Natl Cancer Inst 82:1107–1112

Tayel AA, Sorour NM, El-Baz AF et al (2017) Nano metals appraisal in food preservation and food-related activities. Food preservation. Academic Press, USA, pp 487–526

Vichai V, Kirtikara K (2006) Sulforhodamine B colorimetric assay for cytotoxicity screening. Nat Protoc 13:1112–1116

Wadhwani M, Jain S (2015) Synthesis and antimicrobial activity of ZnS nanoparticles. Res J Recent Sci 4:36–39